# Quantum breathers in capacitively coupled Josephson junctions: Correlations, number conservation, and entanglement

R. A. Pinto and S. Flach
*Max-Planck-Institut für Physik komplexer Systeme, Nöthnitzer Str. 38, 01187 Dresden, Germany*
(Received 26 July 2007; revised manuscript received 6 November 2007; published 17 January 2008)

We consider the classical and quantum dynamics of excitations in a system of two capacitively coupled Josephson junctions. In the classical case the equations of motion admit discrete breather solutions, which are time periodic and localized predominantly on one of the junctions. In the quantum case breather states are found in the central part of the energy spectrum of the confined nonescaping states of the system. We perform a systematic analysis of their tunneling frequency, site correlations, fluctuations of the number of quanta, and entanglement. Quantum breather states show strong site correlation of quanta and are characterized by a strong excitation of quanta on one junction which perform slow coherent tunneling motion from one junction to the other. They suppress fluctuations of the total number of excited quanta. Quantum breather states are the least entangled states among the group of eigenstates in the same range of the energy spectrum. We describe how quantum breather excitations could be experimentally observed by employing the already developed techniques for quantum information processing using Josephson junctions.

DOI: 10.1103/PhysRevB.77.024308 PACS number(s): 63.20.Pw, 74.50.+r, 85.25.Cp, 63.20.Ry

## I. INTRODUCTION

Josephson junctions are the subject of extensive studies in quantum information experiments because they possess two attractive properties: In their classical regime they are nonlinear devices, but also show macroscopic quantum behavior.[1–3] The dynamics of a biased Josephson junction (JJ) is analogous to the dynamics of a particle with a mass proportional to the junction capacitance $C_J$, moving on a tilted washboard potential

$$U(\varphi) = -I_c \frac{\Phi_0}{2\pi} \cos\varphi - I_b \varphi \frac{\Phi_0}{2\pi}, \tag{1}$$

which is sketched in Fig. 1(b). Here $\varphi$ is the phase difference between the macroscopic wave functions in both superconducting electrodes of the junction, $I_b$ is the bias current, $I_c$ is the critical current of the junction, and $\Phi_0 = h/2e$ the flux quantum. When the energy of the particle is large enough to overcome the barrier $\Delta U$ (which depends on the bias current $I_b$) it escapes and moves down the potential, switching the junction into a resistive state with a nonzero voltage proportional to $\dot{\varphi}$ across it. Quantization of the system leads to discrete energy levels inside the potential wells, which are nonequidistant because of the anharmonicity. Note that even if there is not enough energy to classically overcome the barrier, the particle may perform a quantum escape and tunnel outside the well, thus switching the junction into the resistive state.[1] Thus each state inside the well is characterized by a bias and state-dependent lifetime, or its inverse—the escape rate.

Progress on manipulation of quantum JJs includes spectroscopic analysis, better isolation schemes, and simultaneous measurement techniques[2–7] and paves the way for using them as Josephson-junction qubits in arrays for experiments on processing quantum information. Typically the first two or three quantum levels of one junction are used as quantum bits. Since the levels are nonequidistant, they can be separately excited by applying microwave pulses.

However, improvements in experiments manipulating Josephson-junction qubits may have applications beyond the processing of quantum information. Operating the junctions at larger energies in the quantum regime may give rise to other interesting phenomena that nowadays can be experimentally observed by using already developed experimental techniques. For instance, it was suggested that JJs operating at high energies may be used for experiments on quantum chaos.[8–10]

Another interesting phenomenon is the excitation of discrete breathers. They are time-periodic space-localized excitations in anharmonic lattices with translational invariance.[11–14] They localize energy exponentially in space for short-range coupling between lattice sites and have been experimentally observed in such different systems as bond excitations in molecules, lattice vibrations, and spin excitations in solids, electronic currents in coupled JJs, light propagation in interacting optical waveguides, cantilever vibrations in micromechanical arrays, cold atom dynamics in Bose-Einstein condensates loaded on optical lattices, among others.[15–23]

In the quantum regime, quantum breathers[14,24–41] (QBs) appear as nearly degenerate many-quanta bound states. Though being extended in a translationally invariant system, they are characterized by exponentially localized correlation functions in full analogy to their classical counterparts.[30,42] When such states superpose the result is a spatially localized excitation with a very long time to tunnel from one lattice site to another. At variance with the classical case, the evolution of these excitations in time has not been experimentally studied in detail. So far they have been indirectly observed by spectroscopic analysis in molecules and solids.[43–52]

The possibility to directly observe QB excitations evolving in time was addressed by us in a Letter[53] for a system of two capacitively coupled JJs, where by calculating the eigenstates and the spectrum of the system we identified QB states as weakly split tunneling pairs of states.[31–33,37] These eigen-

 

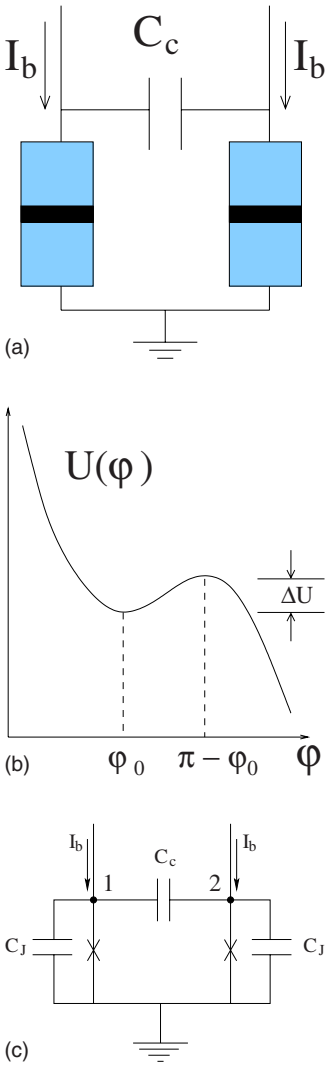


FIG. 1. (Color online) (a) Sketch of the two capacitively coupled Josephson junctions. (b) Sketch of the washboard potential for a single current-biased Josephson-junction. (c) Circuit diagram for two ideal capacitively coupled Josephson junctions.

states appear in the middle of the energy spectrum of the system and are characterized by correlations between the two junctions—if one of them is strongly excited, the other one is not and vice versa. By exciting one of the junctions to a large energy (many quanta), we strongly overlap with QB tunneling states. Consequently we may trap the excitation on the initially excited junction on a time scale which sensitively depends on the amount of energy excited and on the applied bias. We described how QB excitations could be directly observed in time using the available techniques for manipulating JJs in the quantum regime.

In this work we present an extended analysis of the system, performing a systematic and comparative analysis of different properties of QB states. We study their tunneling rates, the site correlations of excited quanta, the fluctuation of the number of excited quanta, and the entanglement of the QB states.

In Sec. II we describe the model for the two coupled JJs[54–56] and briefly consider the classical dynamics, where the equations of motion are numerically solved finding discrete breather solutions. In Sec. III we consider the quantum model and introduce the basis we use to numerically diagonalize the Hamiltonian matrix. We define correlations functions which, together with the energy spectrum, will help us to identify QB states. Then we compute the time evolution of initially localized excitations and relate it to the spectral properties of the system. In Sec. IV we address the fluctuation of the total number of quanta in the eigenstates. In Sec. V we explore the entanglement of the eigenstates. In Sec. VI we describe how QB excitations evolving in time could be experimentally observed and discuss how escaping and decoherence (effects that are not taken into account in the quantum model) would affect the observations. We conclude in Sec. VII.

## II. MODEL AND CLASSICAL DYNAMICS

The system is sketched in Fig. 1(a): Two JJs are coupled by a capacitance $C_c$, and they are biased by the same current $I_b$. The strength of the coupling due to the capacitor is $\zeta = C_c/(C_c + C_J)$.

The Hamiltonian of the system is

$$H = \frac{P_1^2}{2m} + \frac{P_2^2}{2m} + U(\varphi_1) + U(\varphi_2) + \frac{\zeta}{m} P_1 P_2, \tag{2}$$

where

$$m = C_J(1+\zeta)\left(\frac{\Phi_0}{2\pi}\right)^2, \tag{3}$$

$$P_{1,2} = (C_c + C_J)\left(\frac{\Phi_0}{2\pi}\right)^2 (\dot{\varphi}_{1,2} - \zeta \dot{\varphi}_{2,1}). \tag{4}$$

Note that the conjugate momenta $P_{1,2}$ are proportional to the charge at the nodes of the circuit [which are labeled in Fig. 1(c)]. When the junctions are in the superconducting state, they behave like two coupled anharmonic oscillators with plasma frequency $\omega_p(\gamma) = \sqrt{2\pi I_c/\Phi_0 C_J(1+\zeta)}[1-\gamma^2]^{1/4}$, $\gamma = I_b/I_c$ being the normalized bias current. The classical equations of motion are given by

$$\ddot{\varphi}_{1,2} = -\frac{\Phi_0}{2\pi m}(\sin\varphi_{1,2} + \zeta \sin\varphi_{2,1}) + \frac{\Phi_0}{2\pi m}(1+\zeta)\gamma. \tag{5}$$

Despite being invariant under permutation of the junction labels, these equations admit discrete breather solutions,[12] which are time periodic and for which the energy is localized predominantly on one of the junctions (Fig. 2). These orbits can be numerically computed with high accuracy using Newton algorithms.[57,58]

The existence of discrete breathers is possible because the anharmonicity in the JJ potentials makes the frequency of these excitations (and all of their harmonics) nonresonant with the normal modes $\omega_\pm = \sqrt{1 \pm \zeta}\omega_p(\gamma)$ of the coupled-junction system, whose corresponding orbits are delocalized.[12] For the parameters $\gamma = 0.99$ and $\zeta = 0.1$, the normal-mode frequencies are $\omega_+ = 0.394\omega_p(0)$ (in-phase mode) and $\omega_- = 0.356\omega_p(0)$ (out-of-phase mode). The

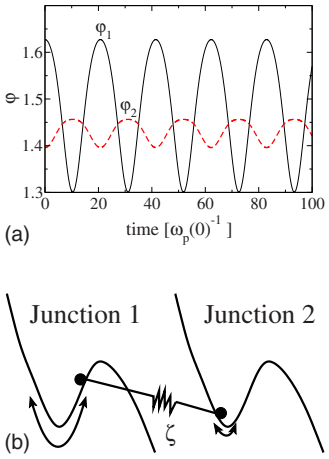


FIG. 2. (Color online) (a) Time evolution of the phase differences and (b) corresponding sketch of an exact discrete breather solution of the equations of motion (5) with frequency $\Omega_b = 0.303\omega_p(0)$ [time is measured in units of the inverse plasma frequency at zero bias $\omega_p(0)^{-1}$]. The parameters are $\gamma=0.99$ and $\zeta=0.1$.

periodic solution shown in Fig. 2 has a frequency below the out-of-phase mode frequency; thus, the discrete breather solution is out of phase as well.

## III. QUANTUM DYNAMICS: EXCITING QUANTUM BREATHER STATES

In the quantum case we compute the energy eigenvalues and the eigenstates of the system. Since we are interested only in the energy transfer between the junctions, we neglect quantum escape for states which will not escape in the classical limit. Thus we use a changed potential energy for the single JJ by adding a hard wall which prevents escape:

$$U_q(\varphi) = \begin{cases} U(\varphi) & \text{if } \varphi \leqslant \pi - \varphi_0, \\ \infty & \text{if } \varphi > \pi - \varphi_0, \end{cases} \tag{6}$$

where $\varphi_0 = \arcsin\gamma$ is the position of the minimum of the potential and $\pi - \varphi_0$ gives the position of the first maximum to the right from the equilibrium position $\varphi_0$ [Fig. 1(b)]. We will later compare the obtained tunneling times with the true state-dependent escape times.

The Hamiltonian of the two-junctions system is given by

$$\hat{H} = \hat{H}_1 + \hat{H}_2 + \zeta\hat{V}, \tag{7}$$

where $\hat{H}_i = \hat{P}_i^2/2m + U_q(\hat{\varphi}_i)$ is the single-junction Hamiltonian and $\hat{V} = \hat{P}_1\hat{P}_2/m$ is the interaction that couples the junctions. The eigenvalues $\varepsilon_{n_i}$ and eigenstates $|n_i\rangle$ of the single-junction Hamiltonian $\hat{H}_i$ were computed by using the Fourier-grid Hamiltonian method.[59] $|n_i\rangle$ is also an eigenstate of the number operator $\hat{n}_i$ with eigenvalue $n_i$. In the harmonic approximation[60]

$$\hat{n}_i = \hat{a}_i^\dagger \hat{a}_i, \tag{8}$$

where $\hat{a}_i^\dagger$ and $\hat{a}_i$ are the bosonic creation and annihilation operators. Since only states with energies below the classical escape energy (barrier) are taken into account, the computed spectra have a finite upper bound. The perturbation $\hat{V}$ does not conserve the total number of quanta $n_1+n_2$, as seen from the dependence of the momentum operators on the bosonic creation and annihilation operators in the harmonic approximation:

$$\hat{P}_{1,2} = (\Phi_0/2\pi)\sqrt{(1+\zeta)C_J\hbar\omega_p/2} \times (\hat{a}_{1,2} - \hat{a}_{1,2}^\dagger)/i. \tag{9}$$

The Hamiltonian matrix is written in the basis of product states of the single-junction problem $\{|n_1,n_2\rangle = |n_1\rangle \otimes |n_2\rangle\}$. The invariance of the Hamiltonian under permutation of the junction labels allows us to use symmetric and antisymmetric basis states

$$|n_1,n_2\rangle_{S,A} = \frac{1}{\sqrt{2}}(|n_1,n_2\rangle \pm |n_2,n_1\rangle) \tag{10}$$

to reduce the full Hamiltonian matrix to two smaller symmetric and antisymmetric decompositions of $\hat{H}$, which after diagonalization respectively give the symmetric and antisymmetric eigenstates of the system.

In order to identify quantum breather states, whose corresponding classical orbits are characterized by energy localization, we define the correlation functions

$$f_\mu(1,2) = \langle \hat{n}_1\hat{n}_2\rangle_\mu, \tag{11}$$

$$f_\mu(1,1) = \langle \hat{n}_1^2\rangle_\mu, \tag{12}$$

where $\langle\hat{A}\rangle_\mu = \langle\chi_\mu|\hat{A}|\chi_\mu\rangle$, $\{|\chi_\mu\rangle\}$ being the set of eigenstates of the system. The ratio $0 \leqslant f_\mu(1,2)/f_\mu(1,1) \leqslant 1$ measures the site correlation of quanta: It is small when quanta are site correlated (i.e., when many quanta are located on one junction there are almost none on the other one) and close to 1 otherwise.

In Fig. 3 we show the nearest-neighbor energy spacing (tunneling splitting) and the correlation function of the eigenstates. For this, and all the rest, we used $I_c = 13.3\ \mu$A,

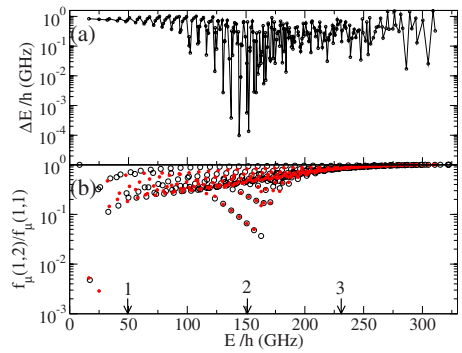


FIG. 3. (Color online) (a) Energy splitting and (b) correlation function vs energy of the eigenstates of the two-junction system (open circles, symmetric eigenstates; solid circles, antisymmetric eigenstates). The labeled arrows mark the energy corresponding to the peak of the spectral intensity in Figs. 4(b), 4(d), and 4(f) (see text). The parameters are $\gamma=0.945$ and $\zeta=0.1$ (22 levels per junction).

$C_J$=4.3 pF, and $\zeta$=0.1, which are typical values in experiments. We see that in the central part of the spectrum the energy splitting becomes small in comparison to the average. The corresponding pairs of eigenstates, which are tunneling pairs, are site correlated and thus QBs. In these states many quanta are localized on one junction and the tunneling time of such an excitation from one junction to the other (given by the inverse energy splitting between the eigenstates of the pair) can be exponentially large and depend sensitively on the number of quanta excited.

Note that the tunneling of quanta between the JJs occurs without an obvious potential energy barrier being present [the interaction between the junctions is only through their momenta, as seen in the Hamiltonian (7)]. This process has been coined *dynamical tunneling*,[61–63] to distinguish from the usual tunneling through a potential barrier. In dynamical tunneling, the barrier—a so-called invariant separatrix manifold—is only visible in phase space, where it separates two regions of regular classical motion between which the tunneling process takes place. Therefore, when referring to the tunneling between the JJs, we implicitly mean that it is dynamical.

The fact that the strongest site-correlated eigenstates occur in the central part of the energy spectrum may be easily explained as follows: Let $N$ be the highest excited state in a single junction, with a corresponding maximum energy $\Delta U$ (Fig. 1). For two junctions the energy of the system with both junctions in the $N$th state is $2\Delta U$, which roughly is the width of the full spectrum. Thus states of the form $|N,0\rangle$ and $|0,N\rangle$ that have energy $\Delta U$ are located approximately in the middle.

Having the eigenvalues and eigenstates, we compute the time evolution of different initially localized excitations and the expectation value of the number of quanta at each junction $\langle \hat{n}_i\rangle(t)=\langle\Psi(t)|\hat{n}_i|\Psi(t)\rangle$. Results are shown in Figs. 4(a), 4(c), and 4(e). We also compute the spectral intensity $I_\mu^0=|\langle\chi_\mu|\Psi_0\rangle|^2$, which measures the strength of overlap of the initial state $|\Psi_0\rangle$ with the eigenstates. Results are shown in Figs. 4(b), 4(d), and 4(f), where we can see a peak in each case, which corresponds to the arrows in Fig. 3(b). We can see that the initial state $|\Psi_0\rangle=|0,5\rangle$ overlaps with eigenstates with an energy splitting between them being relatively large and hence the tunneling time of the initially localized excitation is short. For the case $|\Psi_0\rangle=|0,19\rangle$, QBs are excited: The excitation overlaps strongly with tunneling pairs of eigenstates in the central part of the spectrum, which are site correlated and nearly degenerate. The tunneling time of such an excitation is very long and thus keeps the quanta localized on their initial excitation site for corresponding times. Finally the initial state $|\Psi_0\rangle=|9,19\rangle$ overlaps with weakly site-correlated eigenstates with large energy splitting. Hence the tunneling time is short again.

We computed also the time evolution of the expectation values of the number of quanta for initial conditions which are coherent or incoherent (mixtures) superpositions of product basis states with equal weights. This is relevant for experiments, since it may be hard to excite one junction to a determined state but easier to excite several states of the junction at the same time. We used coherent superpositions (characterized by well-defined states $|\Psi_0\rangle$) and mixtures

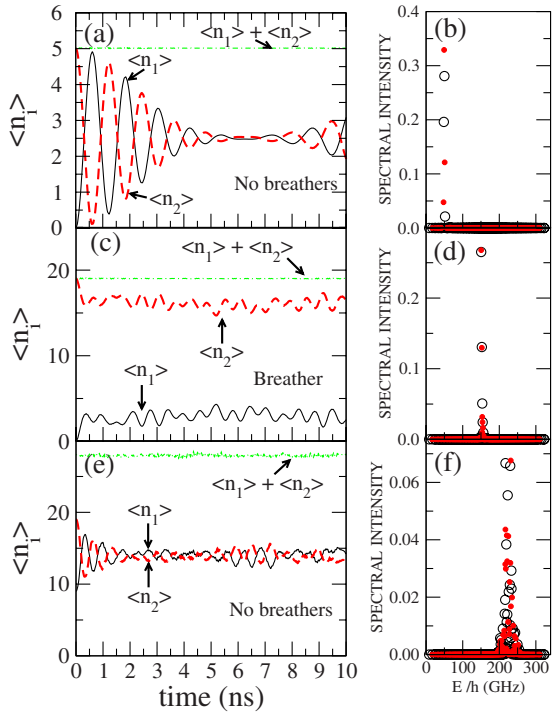


FIG. 4. (Color online) Time evolution of expectation values of the number of quanta at each junction (left panels) for different initial excitations with corresponding spectral intensities (right panels). (a) and (b) $|\Psi_0\rangle=|0,5\rangle$, (c) and (d) $|\Psi_0\rangle=|0,19\rangle$, and (e) and (f) $|\Psi_0\rangle=|9,19\rangle$. Open circles, symmetric eigenstates; solid circles, antisymmetric eigenstates. The energies of the peaks in the spectral intensity are marked by labeled arrows in Fig. 3(b) (see text). The parameters are $\gamma$=0.945 and $\zeta$=0.1 (22 levels per junction).

(characterized by their corresponding density operators $\hat{\rho}_0$) of four basis states around the already used initial states: For the state $|0,5\rangle$ we superposed the basis states $|0,5\rangle$, $|0,6\rangle$, $|0,7\rangle$, and $|0,8\rangle$, for $|0,19\rangle$ the basis states $|0,20\rangle$, $|0,19\rangle$, $|0,18\rangle$, and $|0,17\rangle$, and for $|9,19\rangle$ the basis states $|9,20\rangle$, $|9,19\rangle$, $|9,18\rangle$, and $|9,17\rangle$. Both for superposition and mixture of basis states, the results are qualitatively similar to those shown in Fig. 4. Therefore we expect that some imprecision in exciting an initial state in the junctions would not affect in a relevant way the results. We may also conclude that the excitation of QB states does not rely on the phase coherence. That conclusion will be supported later by the study of entanglement.

Let us estimate how many quanta should be excited in the junctions in order to obtain QBs (tunneling pairs). We compute the density $\rho(n_1,n_2)=|\langle n_1,n_2|\chi\rangle|^2$ of the asymmetric state $|\chi\rangle=(|\chi_b^{(S)}\rangle+|\chi_b^{(A)}\rangle)/\sqrt{2}$, where $|\chi_b^{(S,A)}\rangle$ are the eigenstates belonging to a tunneling pair.[37] In Fig. 5 we show a contour plot of the logarithm of the density for the tunneling pair with energy marked by the arrow labeled by number 2 in Fig. 3(b). We see that the density has its maximum around $n_1$ =19 and $n_2$=0 which is consistent with the result shown in Figs. 4(c) and 4(d) where QBs were excited by using this combination of quanta in the junctions.

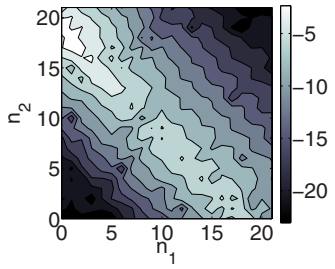


FIG. 5. (Color online) Contour plot of the logarithm of the density of the asymmetric state $|\chi\rangle=(|\chi_b^{(S)}\rangle+|\chi_b^{(A)}\rangle)/\sqrt{2}$ as a function of the number of quanta at junctions 1 and 2 (see text). The parameters are $\gamma=0.945$ and $\zeta=0.1$ (22 levels per junction).

## IV. FLUCTUATIONS OF THE TOTAL NUMBER OF QUANTA

Even though the Hamiltonian does not commute with the total number of quanta, $\hat{N}=\hat{n}_1+\hat{n}_2$, in Figs. 4(a), 4(c), and 4(e), we see that its expectation value has very small fluctuations (less than 1). We can see this approximate conservation of the number of quanta also in the density plotted in Fig. 5, where shows a rim along the line $n_1+n_2=N$ (=19). This might be computationally advantageous when considering larger systems because the strict conservation of $N=n_1+n_2$ would allow us to truncate the Hilbert space and work within a subspace with fixed $N$. Each time the interaction operator $\hat{V}$ acts on a basis state with given $N$, it will generate also states with $N\pm 2$, as can be seen from first-order perturbation theory in $\zeta$ at the harmonic approximation. To study these fluctuations numerically we computed the following weight function for each eigenstate, which measures the relative contribution of all basis states with a given $N$ to the eigenstate under consideration:

$$W_\mu(N)=\sum_{\substack{n_1,n_2\\ n_1+n_2=N}}|\langle n_1,n_2|\chi_\mu\rangle|^2. \tag{13}$$

In Fig. 6 we show the weight function for the three symmetric eigenstates which correspond to the peaks of the spectral

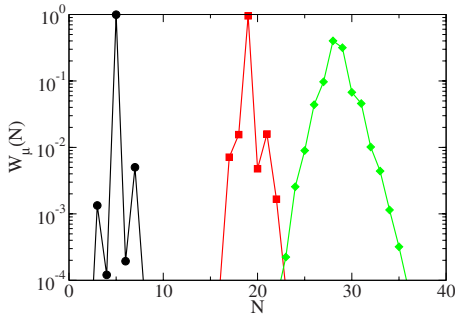


FIG. 6. (Color online) From left to right: weight function as a function of the total number of quanta, $N=n_1+n_2$, for the three symmetric eigenstates at the peaks of the spectral intensities shown in Figs. 4(b), 4(d), and 4(f), respectively. The parameters are $\gamma=0.945$ and $\zeta=0.1$ (22 levels per junction).

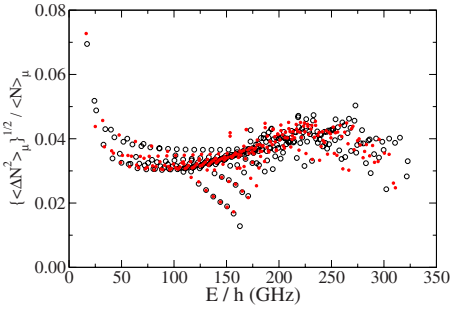


FIG. 7. (Color online) Fluctuation of the total number of quanta for the eigenstates of the coupled-junction system (open circles, symmetric eigenstates; solid circles, antisymmetric eigenstates). The parameters are $\gamma=0.945$ and $\zeta=0.1$ (22 levels per junction).

intensities shown in Figs. 4(b), 4(d), and 4(f), respectively. For the lowest-energy state we can see the expected appearance of two satellite peaks separated by two quanta from the central one. For the higher-energy eigenstates the harmonic approximation does not hold. Most importantly we see that for states in the lower and middle parts of the energy spectrum, the fluctuation of the number of quanta is weak and corresponding states contribute less than 1% to the eigenstate. This is apparently not true at the upper end of the energy spectrum.

Note that the obtained amplitude of fluctuations in the time evolution is much less due to averaging effects and the smallness of the strength of the perturbation $\zeta$. The calculation of $\langle\hat{N}\rangle(t)$ from perturbation theory in the harmonic approximation shows that this quantity oscillates in time with an amplitude that is proportional to $\zeta^2 n_0 m_0$, where $n_0$, and $m_0$ are the energy levels initially excited in the junctions. For $\zeta=0.1$ one finds that the fluctuations are of the order of $10^{-2}$ in the case shown in Fig. 4(a) and of the order of $10^{-1}$ in the cases in Figs. 4(c) and 4(e). Numerical results are consistent with these estimates.

To characterize the variation in the total number of quanta in the eigenstates we computed the fluctuation

$$\sqrt{\langle\Delta N^2\rangle_\mu}=\sqrt{\langle\hat{N}^2\rangle_\mu-\langle\hat{N}\rangle_\mu^2}. \tag{14}$$

In Fig. 7 we plot the relative fluctuation $\sqrt{\langle\Delta N^2\rangle_\mu}/\langle\hat{N}\rangle_\mu$ for the eigenstates, where we can see that it is very small, and for the QB states in the central part of the spectrum it has the smallest values. This follows from the fact that QBs are close to eigenstates having the form

$$|\chi\rangle_{QB}\simeq\frac{1}{\sqrt{2}}(|n,0\rangle\pm|0,n\rangle), \tag{15}$$

with $n\lesssim N$ ($N$ is the number of levels per junctions). These are eigenstates of the total number operator $\hat{N}=\hat{n}_1+\hat{n}_2$, for which the corresponding fluctuations given by Eq. (14) vanish.

## V. ENTANGLEMENT OF QB STATES

Since QB states are close to eigenstates of the $\zeta=0$ case given by (15), one expects that the degree of entanglement in

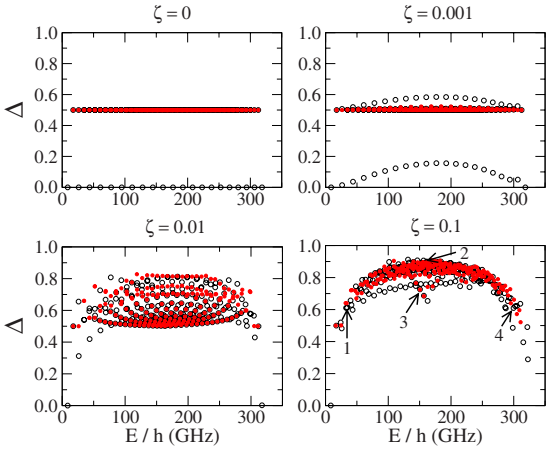


FIG. 8. (Color online) Entanglement of the eigenstates of the coupled-junction system for different values of the coupling strength $\zeta$ (open circles, symmetric eigenstates; solid circles, antisymmetric eigenstates). Here $\gamma=0.945$.

QB states is similar to the degree of entanglement in such states. Since only two basis states are involved, it cannot be a state of maximum entanglement. We measured the degree of entanglement in the eigenstates of the system by minimizing the distance of a given state to the space of product states, which depends on the largest eigenvalue of the reduced density matrix:[64–66]

$$\Delta = \sum_{n_1,n_2}^{N} (\chi^{\mu}_{n_1,n_2} - f_{n_1} g_{n_2})^2, \tag{16}$$

where $\chi^{\mu}_{n_1,n_2}=\langle n_1,n_2|\chi_\mu\rangle$ and the functions $f_{n_1}$ and $g_{n_2}$ are such that $\Delta$ is minimum (see the Appendix for explicit formulas). $\Delta$ measures how far a given eigenstate of the two-junction system is from being a product of single-junction states and has values $0<\Delta<1$ (see the Appendix). For $\zeta=0$ the eigenstates of the system are the basis states given by Eq. (10), where for $n_1=n_2$ it follows that $\Delta=0$ and for $n_1\neq n_2$ [which includes the state in Eq. (15)] $\Delta=0.5$. This measure has a direct relation to the distance of a given eigenstate from a possible one obtained after performing a Hartree approximation.[64]

In a quantum-integrable model with two degrees of freedom[31] it was shown that the region of existence of QB states in the energy spectrum is separated from other states by the energy threshold for which discrete breathers exist in the corresponding classical model. Pairs of eigenstates with energies beyond this threshold show exponentially decreasing energy splitting. In a similar quantum model,[67,68] it was shown that at the mentioned energy threshold the entanglement (using the von Neumann entropy) becomes maximum and then decreases with energy. From these two results we expect that QB states in our case show decreasing entanglement $\Delta$ with energy, tending to 0.5.

In Fig. 8 we show the entanglement of the eigenstates for different values of the coupling strength $\zeta$. For $\zeta=0$ the entanglement has the values 0 and 0.5 corresponding to the basis states with equal and distinct number of quanta at each

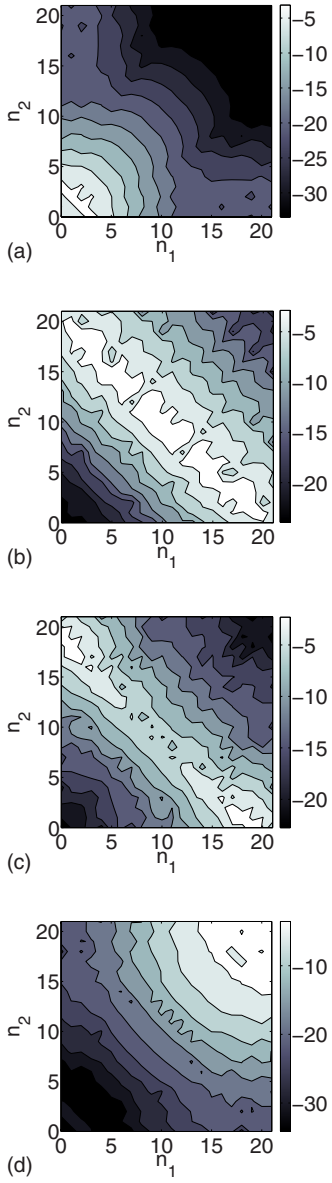


FIG. 9. (Color online) Contour plots of the logarithm of the density of the symmetric eigenstates marked by labeled arrows in Fig. 8 for the case $\zeta=0.1$: (a) S-5 (arrow 1), (b) S-117 (arrow 2), (c) S-95 (arrow 3), and (d) S-246 (arrow 4). The normalized bias current is $\gamma=0.945$ (22 levels per junction).

junction, respectively. When $\zeta>0$ the eigenstates become linear superpositions of the basis states and the entanglement rises, being larger as long as more basis states are involved in building up an eigenstate. This can be seen in Fig. 9, where we plot contours of the density of four symmetric eigenstates marked by labeled arrows in Fig. 8 for $\zeta=0.1$: The low-energy eigenstate marked by the arrow 1 in Fig. 8 consists mainly of a superposition of a few basis states $|n_1,n_2\rangle$ fulfilling $n_1+n_2=3$ as seen in Fig. 9(a); hence, the entanglement is relatively small. When going up in energy the entanglement in the eigenstates quickly increases, becoming maximum in the central part of the energy spectrum and then decreases. An eigenstate in this region of the spectrum like the one marked by the arrow 2 in Fig. 8 involves many basis

states fulfilling $n_1+n_2=20$ [Fig. 9(b)]; hence, the entanglement is large. However, for QB states residing in the same energy region like the one marked by the arrow 3 in Fig. 8, which has the form shown in Eq. (15) as visible in Fig. 9(c), the entanglement is smaller and tends to 0.5 as expected. Finally, high-energy eigenstates like the one marked by the arrow 4 in Fig. 8 involve not so many basis states [Fig. 9(d)]; therefore, the entanglement is also smaller.

We also computed the *von Neumann entropy*[69] (see the Appendix for explicit formulas), which is another standard measure of entanglement, and the results were consistent with those discussed above.

We thus conclude that when QBs appear in a certain part of the energy spectrum, their entanglement drops as compared to the typical entanglement of nearby states. The reason is that QB states predominantly excite two symmetry-related basis states, as opposed to the typical excitation of many other basis states.

## VI. POSSIBLE EXPERIMENTAL OBSERVATION OF QUANTUM BREATHERS

The experimental observation of QBs may be possible by using the scheme of McDermott *et al.* for simultaneous state measurement of coupled Josephson phase qubits,[6] where by applying current pulses in the bias current through each junction the time evolution of the occupation probabilities in the qubits is measured. By applying a microwave pulse on one of the junctions we excite it into a high-energy single-junction state with energy $\varepsilon_l$ and leave the other one in the ground state. In this way we have an initial state similar to the ones shown in Figs. 4(c) and 4(d). After a variable period of time we apply simultaneous current pulses to the junctions to lower their energy barriers $\Delta U$ and enhance the probability of tunneling outside the potential well. Then we test which junction switches to the resistive state (detected by a measurable voltage across it). By repeating the measuring many times we obtain the populations in the junctions as a function of the time between the initial pulse and the simultaneous measuring pulses.

Let us discuss the so far neglected quantum escape. For that we computed $\tau_{escape}$ by using the semiclassical formula[70]

$$\tau_{escape}^{-1}(\varepsilon) = \frac{\omega(\varepsilon)}{2\pi} \exp\left\{-\frac{2}{\hbar}\int_a^b p(\varphi)d\varphi\right\}, \qquad (17)$$

where $a$ and $b$ are the turning points of the classical motion in the reversed potential at $U(\varphi)=\varepsilon$, $p(\varphi)=\sqrt{2[U(\varphi)-\varepsilon]}$, and $\omega(\varepsilon)/2\pi$ is the frequency of the oscillations inside the initial well. In Table I we show the escape time from different metastable states and we compare it with the tunneling time $\tau_{tunnel}$ of an initial excitation $|\Psi(0)\rangle=|0,l\rangle$ between the two junctions, estimated from the energy splitting of the (symmetric-antisymmetric) pair of eigenstates with the largest overlap with the initial excitation. We see that for $l=19$, where we excite QBs, the escape time is long enough for observing at least one tunneling exchange between the two junctions before escaping to the resistive state. Note that the cases $l=18$ and 17 also excite QBs which would show even more tunneling exchanges before escaping. The case $l=16$ does not excite QBs but eigenstates that, though having small energy splitting, do not show strong site correlation of quanta as in the previous cases. From these results we expect that escaping to the resistive state will not prevent from the experimental observation of QB excitations.

TABLE I. Escape times for metastable states in a single Josephson junction $\tau_{escape}$ estimated by formula (17), and the tunneling time of the initial excitation $|\Psi(0)\rangle=|0,l\rangle$ between the two junctions $\tau_{tunnel}$ estimated from energy splittings.

| $l$ | $\tau_{tunnel}$ (ns) | $\tau_{escape}$ (ns) |
|---|---|---|
| 20 | 348 | 42 |
| 19 | $1.8\times10^3$ | $3.5\times10^3$ |
| 18 | $10.16\times10^3$ | $503.2\times10^3$ |
| 17 | $2.3\times10^3$ | $71.2\times10^6$ |
| 16 | 366 | $1.62\times10^9$ |

Another phenomenon that was not taken into account in our quantum model is decoherence. To be able to observe tunneling between the junctions the coherence time has to be longer than the shortest tunneling time between the junctions, which is on the order of 1 ns in the cases shown in Figs. 4(a) and 4(e). In the experiment shown in Ref. 54 using a few levels per junction they obtained a coherence time on the same order. However, in the experiment in Ref. 6 the coherence time was about 25 ns, and more recently in Ref. 7 the coherence time was approximately 80 ns. We expect that further improvements in experiments[5] will give us even longer coherence times.

Note that the above coherence times are shorter than the tunneling times of QB excitations (see Table I); hence, decoherence is an effect that can not be ignored if one wants to do a more realistic quantum description of the system. When exciting a JJ to high-energy states relaxation (over dephasing) is usually the main source of decoherence. We can make a crude estimation of the corresponding relaxation time $T_1$ by using $T_1 \simeq hQ/\varepsilon_l$ ($Q$ is the quality factor of the junctions), which holds for a harmonic potential.[71,72] For $l=19$, 18, and 17, $\varepsilon_l/h$ is around 150 GHz [see Fig. 3(b)]. For the JJs used in Ref. 5, $Q$ is between 500 and 1000, which leads to a relaxation time between 3 ns and 6 ns. It is much smaller than the tunneling time of the QB excitations; therefore, one would expect to see instead of tunneling, a freezing of these excitations on one of the junctions before they decohere due to relaxation.

One could obtain more feasible results by increasing the bias current in such a way that there are less energy levels in the junctions. With this, exciting a QB would need less energy and the relaxation time becomes longer. The tunneling time of that QB excitation is shorter and might be even shorter than the relaxation time, allowing one to observe tunneling before relaxation. This possibility and the inclusion of decoherence in our model are issues that will be addressed in a future work.

## VII. CONCLUSIONS

We have studied the classical and quantum dynamics of high-energy localized excitations in a system of two capaci-

tively coupled JJs. In the classical case the equations of motion admit time-periodic localized excitations (discrete breathers) which can be numerically computed. For the quantum case we showed that excitation of one of the junctions to a high level, leaving the another junction in the ground state, may strongly overlap with QBs (tunneling-pair eigenstates) that reside in the central part of the energy spectrum and localize energy on one of the junctions for a long (tunneling) time. This result would not qualitatively change if we excite a (coherent or incoherent) superposition of several product basis states instead of only one. By using the density function for asymmetric superpositions of QB states one can realize how many quanta can be excited at each junction in order to excite QB states.

In addition to what was described above, the system showed other interesting properties: We found that the system nearly conserves the total number of quanta, which comes from the fact that the coupling between the junctions couples just slightly eigenstates components with different total number of quanta. This opens the possibility to study larger systems without too big computational cost. When computing the fluctuation in the total number of quanta for each eigenstate, QB states show the smallest fluctuations. We showed that entanglement, which reflects how many basis states have significant weight in an eigenstate, increases with energy in most of the eigenstates, becoming maximum at the center of the spectrum and then decreases. QB states from the same energy region are less entangled. This is because a QB state mainly consists of a symmetric or antisymmetric combination of two product basis states localizing many quanta on one of the junctions.

With the available techniques for manipulating Josephson-junction qubits the experimental observation of QB excitations is possible. Escaping to the resistive state of the junctions (which together with decoherence was not taken into account in our quantum model) would not prevent us from doing that, and we expect that improvements on preparation (higher quality factors) and isolation techniques of JJs make it possible to reach long enough coherence times in order to observe the phenomena we described in this work. By changing the parameters of the system (bias current and coupling strength) one could vary the energy, and hence the tunneling time, of a QB excitation with respect to the coherence time, in such a way that it becomes larger than that tunneling time.

## ACKNOWLEDGMENTS

We thank A. Ustinov, J. Lisenfeld, and T. Ohki for useful discussions. This work was supported by the DFG (Grant No. FL200/8) and by the ESF network programme AQDJJ.

## APPENDIX: MEASURES OF ENTANGLEMENT

Let $\mathcal{X} \neq 0$ be a real eigenstate written in a basis of product states $\{|n_1,n_2\rangle\}=\{|n_1\rangle \otimes |n_2\rangle\}$ with $n_1,n_2=1,\ldots,N$. It is a $N \times N$ matrix with elements $\chi_{n_1,n_2}=\langle n_1,n_2|\chi\rangle$. We define the geometric measure of entanglement of this eigenstate by the following quantity:

$$\Delta = \sum_{n_1,n_2}^{N} (\chi_{n_1,n_2} - f_{n_1} g_{n_2})^2, \tag{A1}$$

where the vector functions $\mathbf{f}=(f_1,\ldots,f_{n_1},\ldots)^t$ and $\mathbf{g}=(g_1,\ldots,g_{n_2},\ldots)^t$ are such that $\Delta$ is minimum. The quantity $\Delta$ measures how far the eigenstate is from being a product of functions depending respectively on the numbers $n_1$ and $n_2$.

The minimization of $\Delta$ leads to the formula[64–66]

$$\Delta = \|\mathcal{X}\|^2 - \lambda_{max}, \tag{A2}$$

where $\mathcal{X}$ is a $N \times N$ matrix with elements $\chi_{n_1,n_2}$, $\lambda_{max}$ is the maximum eigenvalue of the $N \times N$ reduced density matrix

$$\mathcal{A} = \mathcal{X}(\mathcal{X})^t, \tag{A3}$$

and $\|\mathcal{X}\|^2=\Sigma_{n_1,n_2}^{N}(\chi_{n_1,n_2})^2$.

Another standard measure of entanglement in the eigenstates is the *von Neumann entropy*, which is used in information theory:[69]

$$S(\hat{\rho}_1) = -\mathrm{Tr}\{\hat{\rho}_1 \log_2 \hat{\rho}_1\} \tag{A4}$$

$$= -\sum_k \lambda_k \log_2(\lambda_k), \tag{A5}$$

where $\log_2$ refers to the logarithm taken in base 2. $\hat{\rho}_1$ is the reduced density operator of either of the subsystems:

$$\hat{\rho}_1 = \mathrm{Tr}_2(\hat{\rho}), \tag{A6}$$

where $\mathrm{Tr}_2$ is the partial trace over the subsystem 2. $\{\lambda_k\}$ is the set of eigenvalues of the reduced density operator $\hat{\rho}_1$.

For the system of coupled JJs an eigenstate has the form

$$|\chi\rangle = \sum_{n_1,n_2}^{N} \chi_{n_1,n_2} |n_1,n_2\rangle. \tag{A7}$$

Then the density operator is

$$\hat{\rho} = |\chi\rangle\langle\chi| \tag{A8}$$

$$= \sum_{n_1,n_2}^{N} \sum_{n_1',n_2'}^{N} \chi_{n_1,n_2} \chi^*_{n_1',n_2'} |n_1,n_2\rangle\langle n_1',n_2'|; \tag{A9}$$

hence, the reduced density operator is

$$\hat{\rho}_1 = \mathrm{Tr}_2(\hat{\rho}) \tag{A10}$$

$$= \sum_{n_1,n_1'}^{N} \left\{ \sum_{n_2}^{N} \chi_{n_1,n_2} \chi^*_{n_1',n_2} \right\} |n_1\rangle\langle n_1'|. \tag{A11}$$

The matrix elements of this reduced operator are

$$\langle n|\hat{\rho}_1|m\rangle = \sum_{n_2}^{N} \chi_{n,n_2} \chi^*_{m,n_2} \tag{A12}$$

$$= A_{n,m}, \tag{A13}$$

where $A_{n,m}$ is a matrix element of $\mathcal{A}$ defined in Eq. (A3). To compute the von Neumann entropy one diagonalizes this matrix and uses Eq. (A5).

Despite the fact that we found similarity in the variation of the two measures when studying QB eigenstates, it is interesting to note that monotonicity does not hold in general; i.e., if one measure is showing that a given state is more strongly entangled than another one, that property may be reversed when using the other measure. The geometric measure is an unambiguous number of the shortest distance from a given state to the subspace of product states, it allows one to reconstruct the optimum product state, and it has a clear relation to the Hartree approximation.[64] For these reasons we presented the numerical results using the geometric measure, rather than the entropy measure.


[1] K. K. Likharev, *Dynamics of Josephson Junctions and Circuits* (Gordon and Breach, Philadelphia, 1984).

[2] *Quantum Computing and Quantum Bits in Mesoscopic Systems*, edited by A. Leggett, B. Ruggiero, and P. Silvestrini (Kluwer Academic, New York, 2004).

[3] *Quantum Entanglement and Information Processing*, 2003 Les Houches Lectures, edited by D. Estève, J. M. Raimond, and J. Dalibard (Elsevier, Amsterdam, 2004).

[4] J. M. Martinis, M. H. Devoret, and J. Clarke, Phys. Rev. Lett. **55**, 1543 (1985).

[5] M. Steffen, M. Ansmann, R. McDermott, N. Katz, R. C. Bialczak, E. Lucero, M. Neeley, E. M. Weig, A. N. Cleland, and J. M. Martinis, Phys. Rev. Lett. **97**, 050502 (2006).

[6] R. McDermott *et al.*, Science **307**, 1299 (2005).

[7] M. Steffen *et al.*, Science **313**, 1423 (2006).

[8] R. Graham, M. Schlautmann, and D. L. Shepelyansky, Phys. Rev. Lett. **67**, 255 (1991).

[9] S. Montangero, A. Romito, G. Benenti, and R. Fazio, Europhys. Lett. **71**, 893 (2005).

[10] E. N. Pozzo and D. Domínguez, Phys. Rev. Lett. **98**, 057006 (2007).

[11] D. K. Campbell, S. Flach, and Y. S. Kivshar, Phys. Today **57** (1), 43 (2004).

[12] S. Flach and C. R. Willis, Phys. Rep. **295**, 181 (1998).

[13] A. J. Sievers and J. B. Page, in *Dynamical Properties of Solids VII, Phonon Physics: The Cutting Edge*, edited by G. K. Horton and A. A. Maradudin (Elsevier, Amsterdam, 1995), p. 137.

[14] S. Aubry, Physica D **103**, 201 (1997).

[15] U. T. Schwarz, L. Q. English, and A. J. Sievers, Phys. Rev. Lett. **83**, 223 (1999).

[16] M. Sato and A. J. Sievers, Nature (London) **432**, 486 (2004).

[17] B. I. Swanson, J. A. Brozik, S. P. Love, G. F. Strouse, A. P. Shreve, A. R. Bishop, W.-Z. Wang, and M. I. Salkola, Phys. Rev. Lett. **82**, 3288 (1999).

[18] E. Trias, J. J. Mazo, and T. P. Orlando, Phys. Rev. Lett. **84**, 741 (2000).

[19] P. Binder, D. Abraimov, A. V. Ustinov, S. Flach, and Y. Zolotaryuk, Phys. Rev. Lett. **84**, 745 (2000).

[20] H. S. Eisenberg, Y. Silberberg, R. Morandotti, A. R. Boyd, and J. S. Aitchison, Phys. Rev. Lett. **81**, 3383 (1998).

[21] J. W. Fleischer, M. Segev, N. K. Efremidis, and D. N. Christodoulides, Nature (London) **422**, 147 (2003).

[22] M. Sato, B. E. Hubbard, A. J. Sievers, B. Ilic, D. A. Czaplewski, and H. G. Craighead, Phys. Rev. Lett. **90**, 044102 (2003).

[23] B. Eiermann, Th. Anker, M. Albiez, M. Taglieber, P. Treutlein, K.-P. Marzlin, and M. K. Oberthaler, Phys. Rev. Lett. **92**, 230401 (2004).

[24] V. Fleurov, Chaos **13**, 676 (2003).

[25] A. C. Scott and J. C. Eilbeck, Phys. Lett. A **119**, 60 (1986).

[26] L. Bernstein, J. C. Eilbeck, and A. C. Scott, Nonlinearity **3**, 293 (1990).

[27] L. J. Bernstein, Physica D **68**, 174 (1993).

[28] E. Wright, J. C. Eilbeck, M. H. Hays, P. D. Miller, and A. C. Scott, Physica D **69**, 18 (1993).

[29] A. C. Scott, J. C. Eilbeck, and H. Gilhøj, Physica D **78**, 194 (1994).

[30] W. Z. Wang, J. T. Gammel, A. R. Bishop, and M. I. Salkola, Phys. Rev. Lett. **76**, 3598 (1996).

[31] S. Aubry, S. Flach, K. Kladko, and E. Olbrich, Phys. Rev. Lett. **76**, 1607 (1996).

[32] S. Flach and V. Fleurov, J. Phys.: Condens. Matter **9**, 7039 (1997).

[33] V. Fleurov, R. Schilling, and S. Flach, Phys. Rev. E **58**, 339 (1998).

[34] G. Kalosakas, A. R. Bishop, and V. M. Kenkre, J. Phys. B **36**, 3233 (2003).

[35] J. Dorignac, J. C. Eilbeck, M. Salerno, and A. C. Scott, Phys. Rev. Lett. **93**, 025504 (2004).

[36] J. C. Eilbeck and F. Palmero, Phys. Lett. A **331**, 201 (2004).

[37] R. A. Pinto and S. Flach, Phys. Rev. A **73**, 022717 (2006).

[38] L. S. Schulman, D. Tolkunov, and E. Mihokova, Phys. Rev. Lett. **96**, 065501 (2006).

[39] L. S. Schulman, D. Tolkunov, and E. Mihóková, Chem. Phys. **322**, 55 (2006).

[40] L. Proville, Physica D **216**, 191 (2006).

[41] Z. Ivić and G. P. Tsironis, Physica D **216**, 200 (2006).

[42] J. C. Eilbeck, in *Localization and Energy Transfer in Nonlinear Systems*, edited by L. Vazquez, R. S. MacKay, and M. P. Zorzano (World Scientific, Singapore, 2003), p. 177.

[43] F. Fillaux and C. J. Carlile, Phys. Rev. B **42**, 5990 (1990).

[44] F. Fillaux, C. J. Carlile, and G. J. Kearley, Phys. Rev. B **58**, 11416 (1998).

[45] L. J. Richter, T. A. Germer, J. P. Sethna, and W. Ho, Phys. Rev. B **38**, 10403 (1988).

[46] P. Guyot-Sionnest, Phys. Rev. Lett. **67**, 2323 (1991).

[47] D. J. Dai and G. E. Ewing, Surf. Sci. **312**, 239 (1994).

[48] R. P. Chin, X. Blase, Y. R. Shen, and S. G. Louie, Europhys. Lett. **30**, 399 (1995).

[49] P. Jakob, Phys. Rev. Lett. **77**, 4229 (1996).

[50] P. Jakob, Appl. Phys. A: Mater. Sci. Process. **75**, 45 (2002).

[51] H. Okuyama, T. Ueda, T. Aruga, and M. Nishijima, Phys. Rev. B **63**, 233404 (2001).

[52] J. Edler, R. Pfister, V. Pouthier, C. Falvo, and P. Hamm, Phys. Rev. Lett. **93**, 106405 (2004).

[53] R. A. Pinto and S. Flach, Europhys. Lett. **79**, 66002 (2007).

[54] A. J. Berkley, H. Xu, R. C. Ramos, M. A. Gubrud, F. W. Strauch, P. R. Johnson, J. R. Anderson, A. J. Dragt, C. J. Lobb, and F. C. Wellstood, Science **300**, 1548 (2003).

[55] P. R. Johnson, F. W. Strauch, A. J. Dragt, R. C. Ramos, C. J. Lobb, J. R. Anderson, and F. C. Wellstood, Phys. Rev. B **67**, 020509(R) (2003).
[56] A. Blais, A. Maassen van den Brink, and A. M. Zagoskin, Phys. Rev. Lett. **90**, 127901 (2003).
[57] S. Flach, in *Energy Localization and Transfer*, edited by T. Dauxois, Anna Litvak-Hinenzon, Robert MacKay, and Anna Spanoudaki (World Scientific, Singapore, 2004), p. 1.
[58] D. Chen, S. Aubry, and G. P. Tsironis, Phys. Rev. Lett. **77**, 4776 (1996).
[59] C. Clay Marston and G. G. Balint-Kurti, J. Chem. Phys. **91**, 3571 (1989).
[60] By harmonic approximation we mean that we use Eqs. (8) and (9) for the number and momentum operators, which hold for the harmonic oscillator potential. For the anharmonic potential of the Josephson junctions these relations do not necessarily hold.
[61] M. Davis and E. Heller, J. Chem. Phys. **75**, 246 (1981).
[62] S. Keshavamurthy, Int. Rev. Phys. Chem. **26**, 521 (2007).
[63] S. Keshavamurthy, J. Chem. Phys. **122**, 114109 (2005).
[64] T.-C. Wei and P. M. Goldbart, Phys. Rev. A **68**, 042307 (2003).
[65] A. Shimony, Ann. N.Y. Acad. Sci. **755**, 675 (1995).
[66] H. Barnum and N. Linden, J. Phys. A **34**, 6787 (2001).
[67] A. P. Tonel, J. Links, and A. Foerster, J. Phys. A **38**, 1235 (2005).
[68] L. B. Fu and J. Liu, Phys. Rev. A **74**, 063614 (2006).
[69] A. P. Hines, R. H. McKenzie, and G. J. Milburn, Phys. Rev. A **67**, 013609 (2003).
[70] L. D. Landau and E. M. Lifshitz, *Quantum Mechanics* (Pergamon, London, 1958).
[71] J. M. Martinis, M. H. Devoret, and J. Clarke, Phys. Rev. B **35**, 4682 (1987).
[72] D. Esteve, M. H. Devoret, and J. M. Martinis, Phys. Rev. B **34**, 158 (1986).